Electronic Supplementary Material (ESI) for ChemComm.

$(H_3O)HCs_2Nb(IO_3)_9$ and $SrNbO(IO_3)_5$: A Facile Synthetic Method of Using Hydrofluoric Acid as Solubilizer

Fei-Fei Mao,[a, b, c] Chun-Li Hu [a], Jin Chen,[a, c] Ru-Ling Tang, [a] Bao-Lin Wu [a, c] and Jiang-Gao Mao*, [a]

[a] *State Key Laboratory of Structural Chemistry, Fujian Institute of Research on the Structure of Matter, Chinese Academy of Sciences, Fuzhou 350002, P. R. China*

[b] *Nanjing Agricultural University, Nanjing 210095, P. R. China.*

[c] *University of the Chinese Academy of Sciences, Beijing 100039, P. R. China*

Table of Contents

Section S1 Materials and Methods

Synthesis.

Cs_2CO_3 (99+%), Nb_2O_5 (99+%), Li_2CO_3 (99+%), $SrCl_2$ (99+%), I_2O_5 (99.0%), HF (40+%, AR) and HNO_3 (65~68%, AR) were used as purchased from Shanghai Reagent Factory. Single crystals of $(H_3O)HCs_2Nb(IO_3)_9$ were obtained hydrothermally from a mixture of Cs_2CO_3(195.5 mg, 0.6 mmol), Li_2CO_3(44.3 mg, 0.6 mmol), Nb_2O_5 (93.0 mg, 0.35 mmol), I_2O_5 (1001.4 mg, 3.0 mmol), 200 μL HF, and 2 mL 3% HNO_3 solution in 25 mL Teflon-lined autoclave, whereas single crystals of $SrNbO(IO_3)_5$ were prepared by hydrothermal reaction of a mixture of $SrCl_2$ (47.6 mg, 0.3 mmol), Nb_2O_5 (93.0 mg, 0.35 mmol), I_2O_5 (834.5 mg, 2.5 mmol), 200 μL HF, and 2 mL H_2O in 25 mL Teflon-lined autoclave. With a lessen amount of HF(<150μL), only $Ba(IO_3)_2(H_2O)$ crystals were obtained; with an increased amount of HF(>300μL), no crystalline phased were synthesized. The autoclaves were heated to 230 ºC in 6 h and held for 3 days, and then cooled to 30 ºC at a rate of 3 ºC/h. Colorless block $(H_3O)HCs_2Nb(IO_3)_9$ and $SrNbO(IO_3)_5$ crystals were collected with a yield of ca. 55% and 50%, respectively (based on Nb). For the syntheses of the two compounds, the initial and final reaction media are very acidic (pH<1). Powder XRD analyses confirmed the purities of the products (Figure S1). The average Cs/Nb/ I and Sr/Nb/ I molar ratios obtained from the EDS elemental analyses are 2.0: 1.0: 8.1 and 1.0: 1.0: 5.1, respectively, which are in good agreement with those obtained from single crystal X-ray diffraction studies.

Instruments and Methods.

Powder X-ray Diffraction.

Powder X-ray diffraction (XRD) patterns were recorded on a Rigaku MiniFlex II diffractometer with graphite-monochromated Cu Kα radiation in the 2θ range of 5−65° with a step size of 0.02°.

Energy-dispersive X-ray spectroscope.

Microprobe elemental analyses and the elemental distribution maps were measured on a field-emission scanning electron microscope (FESEM, JSM6700F) equipped with an energy-dispersive X-ray spectroscope (EDS, Oxford INCA).

Thermal Analysis.

Thermogravimetric analysis (TGA) and differential scanning calorimetry (DSC) were performed with a NETZCH STA 449F3 unit under a N_2 atmosphere, at a heating rate of 10 °C/min.

Optical Measurements

Infrared (IR) spectra were recorded on a Magna 750 FT-IR spectrometer in the form of KBr pellets in the range from 4000 to 400 cm^{-1}. Ultraviolet−visible−near infrared (UV−vis−NIR) spectra in the range of 200−2400 nm were recorded on a PerkinElmer Lambda 950 UV−vis−NIR spectrophotometer. By using *Kubelka-Munk* function,[1] reflectance spectra were converted into absorption spectra.

Second Harmonic Generation Measurements.

Powder SHG measurements were carried out with Q-switch Nd: YAG laser generating radiations at 1064 nm according to Kurtz and Perry method.[2] Crystalline samples in the particle-size range of 150-210 μm were used for SHG measurements. For the phase matching experiments, crystalline $(H_3O)HCs_2Nb(IO_3)_9$ samples were

sieved into distinct particle-size ranges (25-45, 45-53, 53-75, 75-105, 105-150, 150-210 μm). Sieved KDP samples in corresponding particle-size ranges were taken as references for SHG measurements under 1064 nm laser radiation.

Single Crystal Structure Determination.

Single-crystal X-ray diffraction data of the title compound were collected on an Agilent Technologies SuperNova dual-wavelength CCD diffractometer with Mo and Cu Kα radiation (λ = 0.71073 and 1.54178 Å) at 293 K. Data reduction was performed with the program *CrysAlisPro*, and absorption correction based on the multi-scan method was applied.[3] Both structures were solved by direct method and refined by full-matrix least-squares fitting on F^2 using *SHELXL–2018*.[4] All of the non-hydrogen atoms were refined with anisotropic thermal parameters. Both structures were checked for missing symmetry elements using *PLATON* and none was found.[5] The Flack parameter was refined to be -0.02(4) for $(H_3O)HCs_2Nb(IO_3)_9$, indicating that the absolute structure is correct.[6,7] Protons are needed for $(H_3O)HCs_2Nb(IO_3)_9$ to achieve charge balance. Crystallographic data and structure refinements of the two compounds are given in Table S1. More details on the crystallographic data for the two compounds are given in the Tables S2 and S3.

Computational Method.

Single-crystal structural data of $(H_3O)HCs_2Nb(IO_3)_9$ was used for the theoretical calculations. The electronic structures and optical properties calculation were performed using a plane-wave basis set and pseudo-potentials within density functional theory (DFT) implemented in the total-energy code CASTEP.[8,9] For the exchange and

correlation functional, we chose Perdew–Burke–Ernzerhof (PBE) in the generalized gradient approximation (GGA).[10] The interactions between the ionic cores and the electrons were described by the norm-conserving pseudopotential.[11] The following valence-electron configurations were considered in the computation: H-$1s^2$, I-$5s^25p^5$, Nb-$4d^45s^1$, Cs-$5s^25p^66s^1$and O-$2s^22p^4$. The numbers of plane waves included in the basis sets were determined by a cutoff energy of 750eV. Monkhorst-Pack *k*-point sampling of 2 × 3 × 2 was used to perform numerical integration of Brillouin zone. Other parameters and convergent criteria were set as the default values of CASTEP code. During the optical property calculations, approximately 520 empty bands were involved to ensure the convergence of linear optical properties and SHG coefficients. The other parameters and convergent criteria were the default values of CASTEP code.

The calculations of second-order NLO properties were based on length-gauge formalism within the independent-particle approximation.[12] We adopted the Chen's static formula, which was derived by Rashkeev et al.[13] and later improved by Chen's group.[14] The static second-order NLO susceptibility can be expressed as

$\chi^{\alpha\beta\gamma} = \chi^{\alpha\beta\gamma}(\mathrm{VE}) + \chi^{\alpha\beta\gamma}(\mathrm{VH}) + \chi^{\alpha\beta\gamma}(\text{two bands})$

where $\chi^{\alpha\beta\gamma}(\mathrm{VE})$ and $\chi^{\alpha\beta\gamma}(\mathrm{VH})$ give the contributions to $\chi^{\alpha\beta\gamma}$ from virtual-electron processes and virtual-hole processes, respectively; $\chi^{\alpha\beta\gamma}(\text{two bands})$ is the contribution to $\chi^{\alpha\beta\gamma}$ from the two-band processes. The formulas for calculating $\chi^{\alpha\beta\gamma}(\mathrm{VE})$, $\chi^{\alpha\beta\gamma}(\mathrm{VH})$, and $\chi^{\alpha\beta\gamma}(\text{two bands})$ are given in Ref. 14.

References

1 P. Kubelka and F. Munk, *Z. Tech. Physical*, 1931, **12**, 886-892.
2 S. K. Kutz and T. T. Perry, *J. Appl. Phys.*, 1968, **39**, 3798-3813.
3 R. H. Blessing, *Acta Crystallogr. Sect. A*, 1995, **51**, 33-38.
4 G. M. Sheldrick, *Acta Crystallogr. Sect. A*, 2015, **71**, 3-8.
5 A. L. Spek, *J. Appl. Crystallogr*, 2003, **36**, 7-13.
6 H. D. Flack, *Acta Crystallogr. Sect. A*, 1983, **39**, 876-881.
7 H. D. Flack and G. Bernardinelli, *Chirality*, 2008, **20**, 681-690.
8 V. Milman, B. Winkler, J. A. White, C. J. Pickard, M. C. Payne, E. V. Akhmatskaya and R. H. Nobes, *Int. J. Quantum Chem.* , 2000, **77**, 895-910.
9 P. J. D. Lindan, *J. Phys.: Condens. Matter*, 2002, **14**, 2717-2744.
10 J. P. Perdew, K. Burke and M. Ernzerhof, *Phys. Rev. Lett.*, 1996, **77**, 3865-3868.
11 J. S. Lin, A. Qteish, M. C. Payne and V. V. Heine, *Phys. Rev. B*, 1993, **47**, 4174-4180.
12 C. Aversa and J. E. Sipe, *Phys. Rev. B*, 1995, **52**, 14636-14645.
13 S. N. Rashkeev, *Phys. Rev. B*, 1998, **57**, 3905-3919.
14 J. Lin, M. H. Lee, Z. P. Liu, C. T. Chen and C. J. Pickard, *Phys. Rev. B*, 1999, **60**, 13380-13389.

Table S1. Crystallographic Data and structure refinements for $(H_3O)HCs_2Nb(IO_3)_9$ and $SrNbO(IO_3)_5$.

formula	$(H_3O)HCs_2Nb(IO_3)_9$	$SrNbO(IO_3)_5$
Fw	1952.86	1071.03
crystal system	monoclinic	monoclinic
space group	$P2_1$(No. 4)	$P2_1/n$ (No. 14)
T (K)	293(2)	293(2)
a (Å)	12.5917(7)	7.6258(2)
b (Å)	7.9965(4)	18.2110(5)
c (Å)	14.3252(8)	10.6126(3)
β(°)	98.469(6)	92.253(2)
V (Å^3)	1426.67(13)	1472.67(7)
Z	2	2
λ (Mo-K*a*) (Å)	0.71073	1.54178
Dc (g/cm^{-3})	4.546	4.831
μ (mm^{-1})	12.781	94.295
GOF on F^2	1.042	1.042
Flack factor	-0.02(4)	none
R_1 wR_2 [$I > 2\sigma(I)$]	0.0390, 0.0875	0.0415, 0.1023
R_1, wR_2 (all data)	0.0424, 0.0910	0.0543, 0.1134

$R_1 = \Sigma ||F_o| - |F_c|| / \Sigma |F_o|$, $wR_2 = \{ \Sigma w[(F_o)^2 - (F_c)^2]^2 / \Sigma w[(F_o)^2]^2 \}^{1/2}$.

Table S2. Selected bond lengths (Å) for $(H_3O)HCs_2Nb(IO_3)_9$.

Cs(1)-O(14)#1	3.155(11)	Cs(2)-	3.666(10)	I(4)-O(11)	1.774(10)
Cs(1)-O(9)#2	3.157(11)	Cs(2)-	3.722(9)	I(4)-O(12)	1.774(10)
Cs(1)-O(17)	3.234(9)	Cs(2)-	3.749(13)	I(5)-O(13)	1.887(10)
Cs(1)-O(14)#2	3.364(11)	Nb(1)-O(3)	1.932(10)	I(5)-O(14)	1.788(9)
Cs(1)-O(9)#1	3.453(11)	Nb(1)-O(6)	2.027(9)	I(5)-O(15)	1.782(9)
Cs(1)-O(18)	3.465(10)	Nb(1)-O(8)	1.936(9)	I(6)-O(16)	1.876(9)
Cs(1)-O(6)	3.492(10)	Nb(1)-O(10)	1.903(9)	I(6)-O(17)	1.778(9)
Cs(1)-O(7)#1	3.602(13)	Nb(1)-O(13)	1.969(9)	I(6)-O(18)	1.835(9)
Cs(1)-O(13)#2	3.621(8)	Nb(1)-O(16)	1.964(9)	I(7)-O(19)	1.817(10)
Cs(1)-O(13)	3.751(9)	I(1)-O(1)	1.804(8)	I(7)-O(20)	1.816(9)
Cs(1)-O(5)#2	3.774(12)	I(1)-O(2)	1.795(9)	I(7)-O(21)	1.815(10)
Cs(2)-O(7)#1	3.106(10)	I(1)-O(3)	1.910(10)	I(8)-O(22)	1.802(9)
Cs(2)-O(11)#3	3.139(11)	I(2)-O(4)	1.796(9)	I(8)-O(23)	1.792(9)
Cs(2)-O(1)#3	3.154(10)	I(2)-O(5)	1.794(9)	I(8)-O(24)	1.888(11)
Cs(2)-O(1)#1	3.238(11)	I(2)-O(6)	1.851(9)	I(9)-O(25)	1.825(10)
Cs(2)-O(17)	3.376(11)	I(3)-O(7)	1.789(10)	I(9)-O(26)	1.803(10)
Cs(2)-O(2)#1	3.400(10)	I(3)-O(8)	1.879(9)	I(9)-O(27)	1.804(10)
Cs(2)-O(16)	3.497(10)	I(3)-O(9)	1.774(10)		
Cs(2)-O(11)#1	3.522(11)	I(4)-O(10)	1.914(9)		

Symmetry transformations used to generate equivalent atoms: #1 x, y-1, z; #2 -x+1, y-1/2, -z+2; #3 -x+1, y-1/2, -z+1.

Table S3. Selected bond lengths (Å) for $SrNbO(IO_3)_5$.

Sr(1)-O(8)#1	2.558(10)	I(1)-O(1)	1.827(9)
Sr(1)-O(5)#2	2.563(9)	I(1)-O(2)	1.816(10)
Sr(1)-O(9)	2.580(9)	I(1)-O(3)	1.783(10)
Sr(1)-O(10)#3	2.645(10)	I(2)-O(4)	1.885(8)
Sr(1)-O(2)#4	2.677(9)	I(2)-O(5)	1.787(10)
Sr(1)-O(6)#5	2.693(9)	I(2)-O(6)	1.808(9)
Sr(1)-O(3)#6	2.723(10)	I(3)-O(7)	1.883(10)
Sr(1)-O(15)#2	2.749(10)	I(3)-O(8)	1.758(10)
Sr(1)-O(11)#7	2.848(10)	I(3)-O(9)	1.792(10)
Nb(1)-O(16)	1.734(10)	I(4)-O(10)	1.763(11)
Nb(1)-O(7)	1.965(9)	I(4)-O(11)	1.800(8)
Nb(1)-O(12)	1.973(10)	I(4)-O(12)	1.867(10)
Nb(1)-O(4)	2.056(9)	I(5)-O(13)	1.864(8)
Nb(1)-O(1)	2.072(10)	I(5)-O(14)	1.783(10)
Nb(1)-O(13)	2.170(9)	I(5)-O(15)	1.794(10)

Symmetry transformations used to generate equivalent atoms: #1 x-1/2, -y+1/2, z-1/2; #2 -x+1, -y, -z+1; #3 -x+1/2, y+1/2, -z+1/2; #4 x, y, z-1; #5 -x+1/2, y+1/2, -z+3/2; #6 x+1/2, -y+1/2, z-1/2; #7 -x, -y, -z+1.

Table S4. Calculation of dipole moment for IO_3 polyhedra and net dipole moment for a unit cell and the dipole moment per unit volume in $(H_3O)HCs_2Nb(IO_3)_9$.

$(H_3O)HCs_2Nb(IO_3)_9$				
Polar unit	Dipole moment (D = Debyes.)			
	a-component	*b*-component	*c*-component	total magnitude
$I(1)O_3$	±10.80	10.84	±2.22	15.47
$I(2)O_3$	±3.33	13.22	±8.23	15.93
$I(3)O_3$	±15.61	6.31	±1.08	16.87
$I(4)O_3$	±11.71	-9.25	±6.86	16.43
$I(5)O_3$	±9.31	11.37	±6.86	15.01
$I(6)O_3$	±8.42	-3.01	±13.43	16.14
$I(7)O_3$	±11.69	-3.6	±7.92	14.58
$I(8)O_3$	±0.96	-14.98	±3.59	15.43
$I(9)O_3$	±14.86	2.74	±3.54	15.52
NbO_6	0.44	-0.18	1.09	1.19
Net dipole moment (a unit cell, Z=2)	0.88	26.92	2.18	27.06

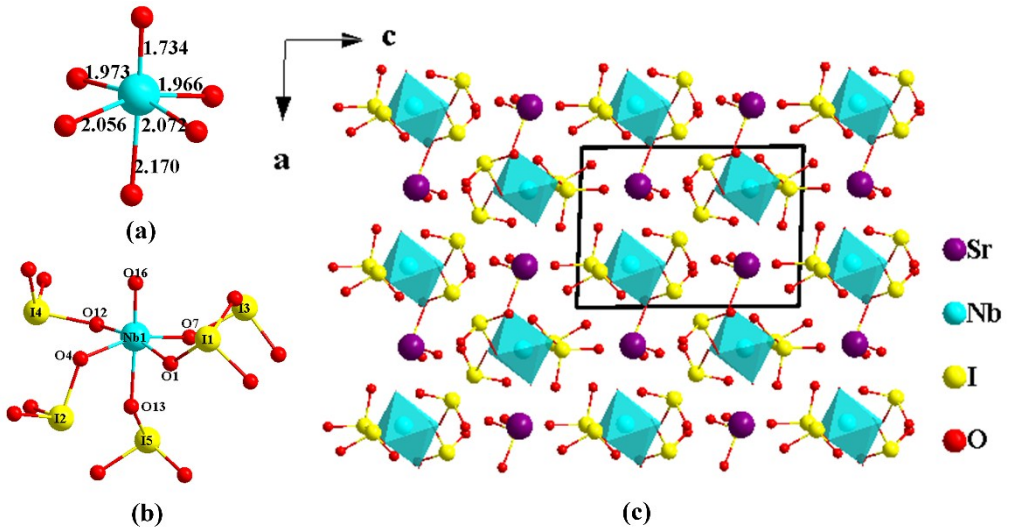

Fig. S1. The NbO_6 octahedron (a), the coordination geometry around the Nb^{5+} cation (b), and view of the structure of $SrNbO(IO_3)_5$ down the *b*-axis (c).

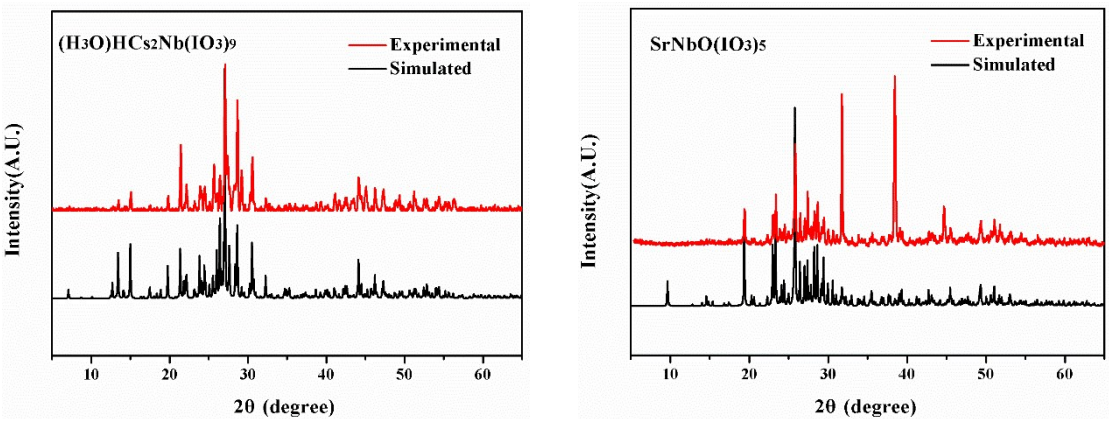

(a) **(b)**

Fig. S2. Simulated and measured powder X-ray diffraction patterns of $(H_3O)HCs_2Nb(IO_3)_9$ (a) and $SrNbO(IO_3)_5$ (b).

Thermal Analysis. Thermogravimetric analysis (TGA) indicates that $(H_3O)HCs_2Nb(IO_3)_9$ and $SrNbO(IO_3)_5$ exhibit different thermal behaviors. The two compounds are thermally stable up to 137, and 123 °C, respectively (Figure S3). After dehydration in the temperature region of 137 ~ 210 °C, $(H_3O)HCs_2Nb(IO_3)_9$ quickly lost weight in the temperature region of 210 ~ 585 °C, showing two steps of weight losses. An endothermic peak was observed at 557 °C in the DSC curve. The weight losses corresponds to the release of I_2, O_2 and H_2O, and the experimental and calculated values are given in Figure S3a. The sample of $SrNbO(IO_3)_5$ gradually lost weight in the temperature region of 123 ~ 610 °C, and showed one step of weight losses. Endothermic peak was observed at 461 °C in the DSC curve. These weight losses correspond to the release of I_2 and O_2, and the experimental and calculated values are given in Figure S3b.

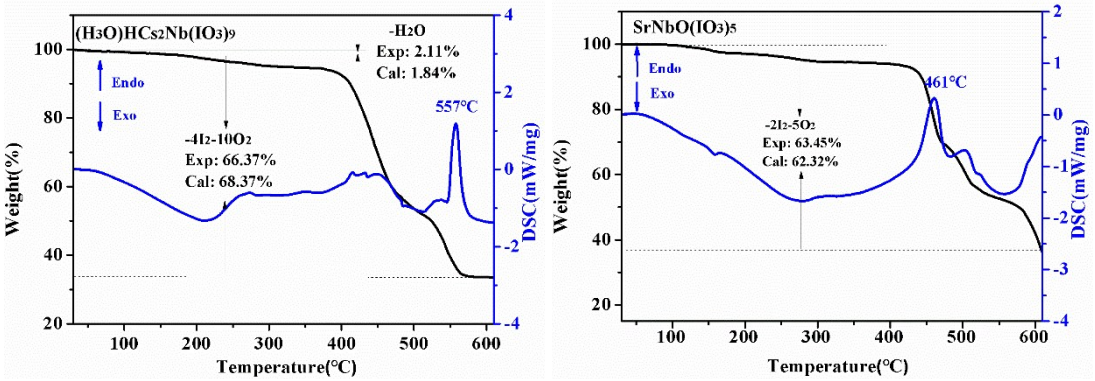

(a) **(b)**

Fig. S3. TGA and DSC curves of $(H_3O)HCs_2Nb(IO_3)_9$ (a) and $SrNbO(IO_3)_5$ (b) under a N_2 atmosphere.

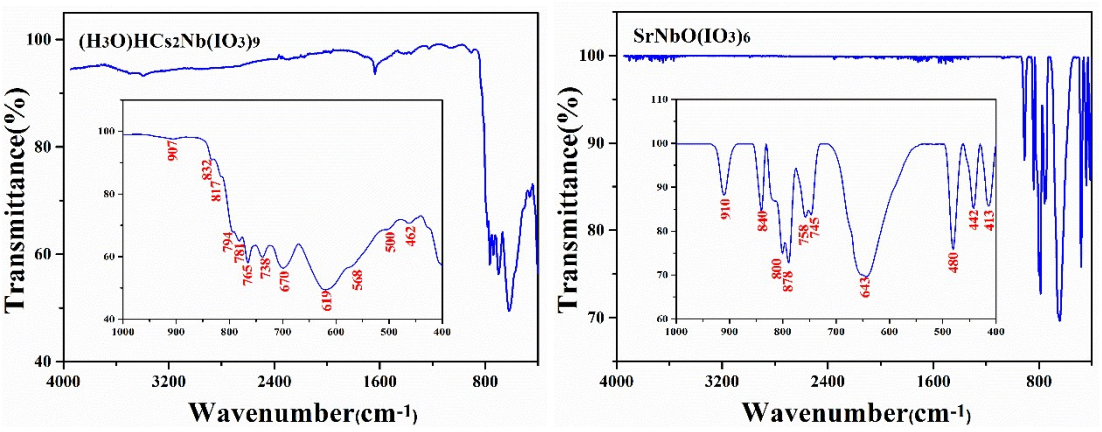

Fig. S4. IR spectra of $(H_3O)HCs_2Nb(IO_3)_9$ (a) and $SrNbO(IO_3)_5$ (b).

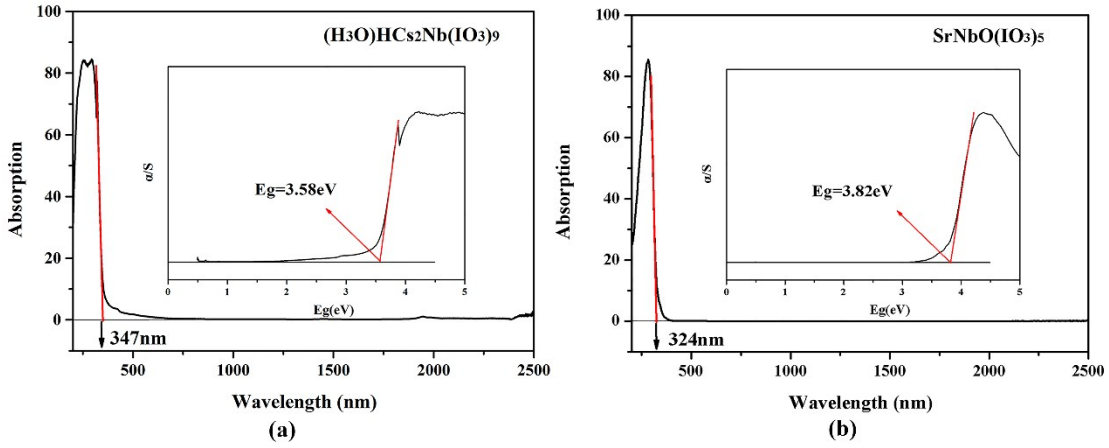

Fig. S5. UV-vis-IR spectra of $(H_3O)HCs_2Nb(IO_3)_9$ (a) and $SrNbO(IO_3)_5$ (b).

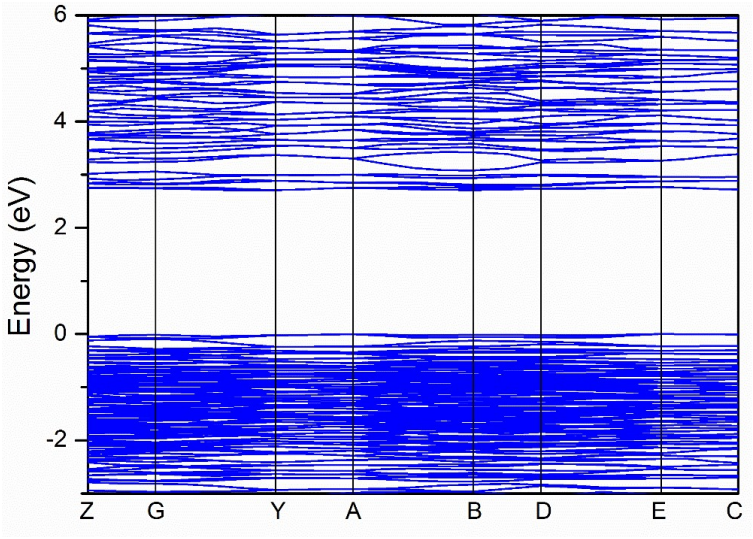

Fig. S6. The calculated band structure of $(H_3O)HCs_2Nb(IO_3)_9$.

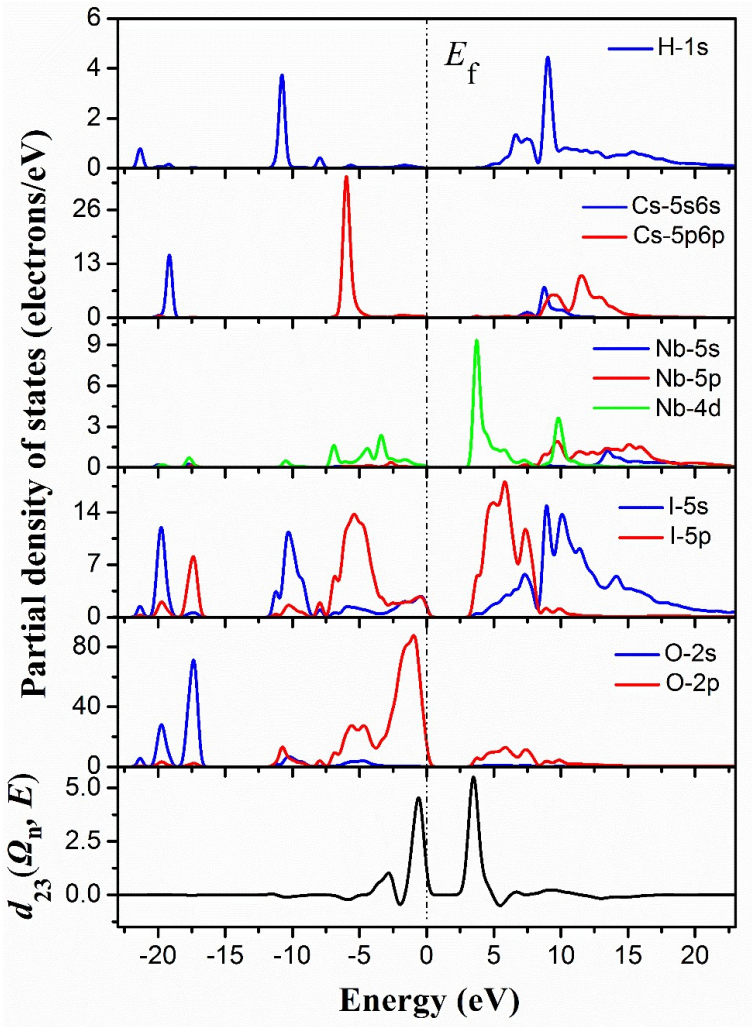

Fig. S7. The scissor-added partial density of states for $(H_3O)HCs_2Nb(IO_3)_9$.

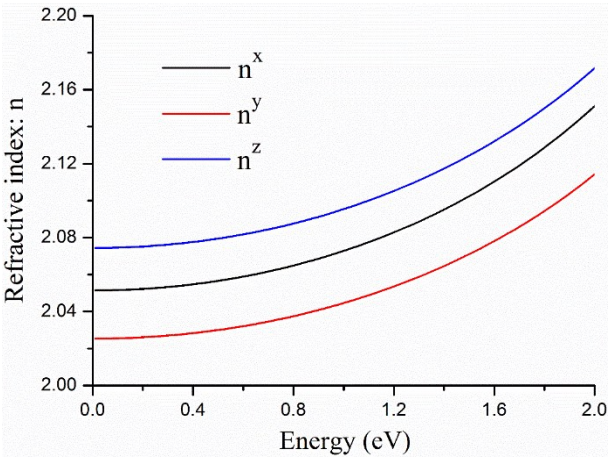

Fig. S8. Calculated refractive indexes for $(H_3O)HCs_2Nb(IO_3)_9$.